

X-ray scattering from surfaces: discrete and continuous components of roughness

Darren Dale,^{1,2} Aaron Fleet,^{3,2,†} Y. Suzuki,⁴ and J. D. Brock^{3,2}

¹*Department of Materials Science and Engineering,
Cornell University, Ithaca, New York 14853, USA*

²*Cornell Center for Materials Research,
Cornell University, Ithaca, New York 14853, USA*

³*School of Applied and Engineering Physics,
Cornell University, Ithaca, New York 14853, USA*

⁴*Department of Materials Science and Engineering,
UC Berkeley, Berkeley, California 94720, USA*

(Dated: March 23, 2022)

Abstract

Incoherent surface scattering yields a statistical description of the surface, due to the ensemble averaging over many independently sampled volumes. Depending on the state of the surface and direction of the scattering vector relative to the surface normal, the height distribution is discrete, continuous, or a combination of the two. We present a treatment for the influence of multimodal surface height distributions on Crystal Truncation Rod scattering. The effects of a multimodal height distribution are especially evident during *in-situ* monitoring of layer-by-layer thin-film growth via Pulsed Laser Deposition. We model the total height distribution as a convolution of discrete and continuous components, resulting in a broadly applicable parameterization of surface roughness which can be applied to other scattering probes, such as electrons and neutrons. Convolution of such distributions could potentially be applied to interface or chemical scattering. Here we find that this analysis describes accurately our experimental studies of h001 in SrTiO₃ annealing and homoepitaxial growth.

PACS numbers: 61.10.-i, 61.10.Kw, 68.37.Ps, 68.47.Gh, 68.55.Ac, 81.15.Fg

Keywords: Crystal truncation rods, film growth, pulsed deposition, surface roughness, SrTiO₃, surface scattering, X-ray diffraction, X-ray scattering

I. INTRODUCTION

The interaction of a scattering probe with a smooth, crystalline surface gives rise to streaks of intensity in reciprocal space known as Crystal Truncation Rods (CTRs). CTR intensity is sensitive to atomic-scale surface roughness such as the oscillatory surface roughness that arises during the so-called layer-by-layer¹ or polynuclear growth^{2,3,4}. Reflection High Energy Electron Diffraction (RHEED) is one example of a technique that is often used for *in-situ* monitoring of film growth via CTR intensity.^{5,6,7,8,9} Recently, the large monochromatic flux available from synchrotron sources ($\sim 10^{13}$ photons/second) have enabled time-resolved *in-situ* X-ray scattering studies of film growth as well.^{10,11,12,13,14,15,16,17,18,19,20} These *in-situ* scattering techniques enable materials engineering at the atomic level via the carefully controlled deposition of sequences of single atomic layers.^{21,22,23,24}

Growth of complex oxide thin films with atomic-scale control via scattering-based *in-situ* monitoring has recently drawn intense interest. This is due in part to the broad range of materials properties that are manifest with changes in stoichiometry, even within a single structure family. Pulsed Laser Deposition (PLD) is an attractive growth technique for such epitaxial complex oxide films and heterostructures, due to its ability to transfer complex stoichiometries from the target to the film. Many interesting phenomena have recently been reported, including metallic behavior at the interface between two band insulators in SrTiO₃/LaAlO₃ heterostructures⁵, superconductivity in BaCuO₂/SrCuO₂ heterostructures²⁵ (neither BaCuO₂ nor SrCuO₂ are superconducting in bulk), ferroelectricity in SrZrO₃/SrTiO₃ heterostructures²⁶ (neither SrZrO₃ nor SrTiO₃ is ferroelectric in bulk), and enhanced ferroelectric polarization in CaTiO₃/SrTiO₃/BaTiO₃ heterostructures²⁷.

Despite the increasing popularity of scattering probes as a method for investigating growth, the problem of directly comparing models of growth kinetics to scattering data remains a challenge. Such a comparison requires descriptions of the surface and the resulting scattered intensity that are complex enough to capture the physics of the problem, yet simple enough to lend themselves to, for example, least squares fitting. The influence of surface roughness on X-ray intensity can be readily calculated for Gaussian roughness²⁸ or discrete roughness on the order of the out-of-plane lattice spacing²⁹ such as arises during nearly ideal layer-by-layer growth, but we require a more generally applicable model to analyze the evolution between these two limits. Previous reports have modeled continuous or discrete roughness independently of one another,³⁰ but real crystal surfaces have a miscut, and therefore have concomitant discrete and continuous components of

surface roughness.

Here, we treat the overall surface roughness as a convolution of discrete binomial and continuous Gaussian distributions, which results in a simple parameterization that is broadly applicable. We show that the X-ray intensity along the CTR associated with reciprocal lattice point \mathbf{G} can be written in a simple, closed-form solution as

$$\frac{I^{\mathbf{G}}(\mathbf{Q})}{I_0^{\mathbf{G}}(\mathbf{Q})} = \frac{1}{4p(1-p)} \sin^2 \left(\frac{Q_z c^0}{2} \right) e^{-\sigma_c^2 (Q_z - G_z)^2};$$

where c^0 is the discrete step height, n and p are the usual parameters in the binomial distribution, and σ_c is the continuous RMS roughness. We present the application of this model to our studies of *in-situ* X-ray scattering during annealing of r001-SrTiO_3 and subsequent homoepitaxial growth via PLD, and find that our data is accurately described by a simple model for the dependence of σ_c , n and p with film thickness.

II. THEORY

In this report, we present a closed form solution of the kinematic scattering theory for surfaces with roughness that is continuous, discrete, or a combination of the two. We begin by assuming that the first Born approximation is valid, i.e. scattering geometries that do not coincide with Bragg conditions. The scattered intensity can be written in the form $I(\mathbf{Q}) = C(\mathbf{Q}) \mathcal{A}(\mathbf{Q})^2$, where $C(\mathbf{Q})$ is a prefactor associated with the scattering geometry, polarization, volume of the unit cell, and scattering cross-section.^{31,32,33} Assuming no surface reconstruction, the scattered intensity for a miscut crystal can be calculated by explicitly performing the kinematic sums:

$$I(\mathbf{Q}) = \sum_N C(\mathbf{Q}) \sum_{\mathbf{r} \in \mathbf{s}_k} \frac{F_{\text{sub}}(\mathbf{Q}) e^{i\mathbf{Q} \cdot \mathbf{R}(\mathbf{s}_k)}}{1 - e^{iQ_z c_0}}^2; \quad (1)$$

where $\hbar\mathbf{Q}$ is the momentum transfer, $F_{\text{sub}}(\mathbf{Q})$ is the structure factor of the substrate, c_0 is the out-of-plane lattice parameter, \mathbf{s}_k is a vector in the plane of the average surface, $\mathbf{R}(\mathbf{s}_k)$ is the position of the surface, $\sum_{\mathbf{r} \in \mathbf{s}_k}$ is a sum over surface positions in each coherently illuminated region, and \sum_N is a sum over coherent regions. X-ray scattering measurements can be classified as either coherent, partially coherent, or incoherent, depending on the size and coherence volume of the X-ray beam. Coherent scattering probes a single realization of the surface ($N = 1$), while incoherent scattering probes the statistical behavior of an ensemble of realizations. This report will focus on incoherent

scattering measurements. A simulated reciprocal-space map of the incoherent scattering intensity for an $\text{h}001$ -oriented SrTiO_3 crystal with 0.198° miscut is presented in figure 1-(a). When the terrace size is small relative to the transverse coherence length, each reciprocal lattice point \mathbf{G} has an associated CTR oriented parallel to the surface normal of the average surface. Figure 1-(b) compares experimental K -scan data ($H = 0, L = 0.5$) with the model. The dominant peaks are associated with the $\text{h}001$ and $\text{h}00\bar{1}$ CTRs, and satellites can be observed which correspond to the $\text{h}00\bar{1}$ and $\text{h}002$ rods. Note also the weak diffuse scattering, which is associated with irregularities in the terrace size and thermal diffuse scattering.

While such brute-force calculations are illuminating, they are quite computationally intensive. Alternatively, statistical approaches can be used. Assuming translational invariance, it has previously been shown that the scattering intensity of a CTR associated with reciprocal lattice point \mathbf{G} can in general be written for any surface height distribution^{34,35}

$$I_{total} \propto \sum_{\mathbf{s}_k, \mathbf{g}} \sum_{\mathbf{s}_k^0, \mathbf{g}^0} e^{i(\mathbf{Q} - \mathbf{G}) \cdot (\mathbf{s}_k - \mathbf{s}_k^0)} e^{i(Q_z - G_z)h(\mathbf{s}_k) - h(\mathbf{s}_k^0)}; \quad (2)$$

where $\mathbf{s}_k - \mathbf{s}_k^0$ is the in-plane vector between scatterers, $Q_z - G_z = (\mathbf{Q} - \mathbf{G}) \cdot \hat{\mathbf{n}}$, $h = \mathbf{r} \cdot \hat{\mathbf{n}}$ is the surface height as measured along the surface normal (as opposed to the terrace normal), and $e^{i(Q_z - G_z)h(\mathbf{s}_k) - h(\mathbf{s}_k^0)}$ is the height difference function.

Previous theoretical investigations, primarily for two-level systems such as ideal layer-by-layer growth on crystals without miscut, have shown that the total scattering intensity can be split into the sum of CTR and diffuse components $I_{total} = I_{CTR} + I_{diffuse}$.^{29,36,37,38} This statistical interpretation of scattering has enabled extensive studies of thin-film growth.³⁰

Here we focus on the CTR scattering intensity associated with reciprocal lattice point \mathbf{G} , which may be either specular or off-specular. Given $\Delta h(\mathbf{s}_k) = h(\mathbf{s}_k) - \langle h \rangle$, we assume delta-correlated height fluctuations $\langle \Delta h(\mathbf{s}_k) \Delta h(\mathbf{s}_k^0) \rangle = \sigma^2 \delta(\mathbf{s}_k - \mathbf{s}_k^0)$ such that

$$I^{\mathbf{G}}(\mathbf{Q}) = I_0^{\mathbf{G}}(\mathbf{Q}) e^{-(Q_z - G_z)^2 \sigma^2}; \quad (3)$$

For a Gaussian surface height distribution, the scattering intensity can be simplified to yield the familiar result

$$I^{\mathbf{G}}(\mathbf{Q}) = I_0^{\mathbf{G}}(\mathbf{Q}) e^{-(Q_z - G_z)^2 \sigma^2}; \quad (4)$$

For a flat crystal without miscut, the ideal intensity is³⁵

$$I_0^{\mathbf{G}}(\mathbf{Q}) = C(\mathbf{Q}) \frac{F_{sub}(\mathbf{Q})^2 \delta^{(2)}(\mathbf{Q}_k - \mathbf{G}_k)}{\sin^2 \frac{Q_z c_0}{2}}; \quad (5)$$

For a crystal with a miscut that yields a surface normal along $\hat{\mathbf{n}}$, the ideal intensity (which neglects the surface roughness associated with the miscut itself), is

$$I_0^{\mathbf{G}}(\mathbf{Q}) = C(\mathbf{Q}) \frac{F_{\text{sub}}(\mathbf{Q})^2 \delta^{(2)}[(\mathbf{Q} - \mathbf{G}) \cdot \hat{\mathbf{n}}]}{(Q_{\parallel} - G_{\parallel})^2} \quad (6)$$

An Atomic Force Microscopy (AFM) image of a $\text{h}001$ SrTiO_3 surface is shown in figure 2-(a). The existence of a miscut, with irregular terrace sizes, produces a Gaussian height distribution, and the resulting X-ray intensity can therefore be described by equation 4. Many surfaces, however, have more complicated height distributions. PLD, for example, results in the nucleation, growth, and coalescence of many small, two-dimensional islands on the surface. Previous *in-situ* studies of PLD growth have shown that material that deposits on one of these small islands tends to diffuse to the step edge and incorporate into the underlying layer,^{10,11,15} enabling extended smooth growth. A simulation of the surface shown in figure 2-(a) after depositing one half monolayer via layer-by-layer growth is shown in figure 2-(b). The system has evolved such that a bimodal distribution exists. Therefore, the surface height distribution has both continuous and discrete character. The discussion that follows is motivated by the need of a model that can handle the effect of such a surface height distribution on the scattered intensity.

In order to proceed, it is instructive to consider a special case: an ideally flat crystal with zero miscut and initial CTR intensity $I_0^{\mathbf{G}}(\mathbf{Q})$. We then assume random, pulsed deposition where material does not deposit on the same site twice in a single pulse, and no surface diffusion occurs after adsorption. The surface height distribution is then given by the well-known binomial distribution:

$$P_d(h) = \sum_k \binom{n}{k} p^k (1-p)^{n-k} \delta(h - kc^0); \quad (7)$$

where n is the number of pulses, p is the fraction of the surface covered with new material during a single pulse, c^0 is the step height and k is an index of overlayers. The mean is $\langle h \rangle = npc^0$ and the RMS surface roughness is $\sigma_d = c^0 \sqrt{np(1-p)}$. The expectation value in equation 3 can be simplified, using the binomial theorem:

$$\begin{aligned} \int_{-\infty}^{\infty} e^{i(\mathbf{Q}_{\parallel} - \mathbf{G}_{\parallel})h} P_d(h) dh &= \int_{-\infty}^{\infty} P_d(h) e^{i(\mathbf{Q}_{\parallel} - \mathbf{G}_{\parallel})h} dh \\ &= \sum_{k=0}^n \binom{n}{k} (p e^{i(\mathbf{Q}_{\parallel} - \mathbf{G}_{\parallel})c^0})^k (1-p)^{n-k} \\ &= [1 - p + p e^{i(\mathbf{Q}_{\parallel} - \mathbf{G}_{\parallel})c^0}]^n; \end{aligned} \quad (8)$$

The scattering intensity from a surface with a binomial height distribution is therefore

$$\frac{I^G(\mathbf{Q})}{I_0^G(\mathbf{Q})} = \left[1 - 4p(1-p)\sin^2\left(\frac{(Q_z - G_z)c^0}{2}\right) \right]^n : \quad (9)$$

Alternatively, this result can be derived by performing a sum of the overlayers, as described by Robinson,³⁹ and illustrated in appendix A. There it is shown for the more general case where the amount of material that adsorbs during each pulse may vary, that the intensity after n pulses is

$$\frac{I^G(\mathbf{Q})}{I_0^G(\mathbf{Q})} = \prod_n \left[1 - 4p_n(1-p_n)\sin^2\left(\frac{(Q_z - G_z)c^0}{2}\right) \right] : \quad (10)$$

This more flexible description of the surface comes at the expense of additional parameters. In figure 3, three CTR intensity profiles for $\text{h}001\text{SrTiO}_3$ are simulated: an ideally flat substrate; a sample with $n = 1$, $p = 0.5$, $\sigma_d = 1.95\text{\AA}$; and a sample with $n = 25$, $p = 0.01$ and $\sigma_d = 1.94\text{\AA}$. The CTR intensity is most sensitive to the surface roughness in the so-called anti-Bragg scattering geometries, where $Q_z = \frac{m\pi}{c^0}$; $m = 1, 3, 5, \dots$. Figure 3 illustrates that the RMS surface roughness itself is not always sufficient to describe the surface statistically, since the two surfaces with nearly identical total roughness have very different CTR profiles. The n, p parameterization provides the additional information necessary to model discrete surface roughness on the order of the out-of-plane lattice spacing.

Equation 9 can be rearranged, and by substituting $n = \frac{\sigma_d^2}{p(1-p)c^0} \log_e \left[1 - 4p(1-p)\sin^2\left(\frac{(Q_z - G_z)c^0}{2}\right) \right]$, we arrive at an expression that describes how the scattered intensity varies with σ_d, Q_z and p :

$$\frac{I^G(\mathbf{Q})}{I_0^G(\mathbf{Q})} = \exp \left[-\frac{\sigma_d^2}{p(1-p)c^0} \log_e \left[1 - 4p(1-p)\sin^2\left(\frac{(Q_z - G_z)c^0}{2}\right) \right] \right] : \quad (11)$$

In the limit of $Q_z \rightarrow G_z$, equation 11 can be approximated using first order Taylor expansions, $\sin^2(x) \approx x^2/2$, $\log_e(1-x) \approx -x$. First expanding $\sin^2(x)$, the expansion of the resulting log yields a simplified form of equation 11, which is independent of p and identical to the Gaussian roughness dependence in equation 4.

Alternatively, in the limit of $p \rightarrow 0$, the log in equation 11 can be approximated regardless of the value of Q_z . In this limit, the binomial distribution exhibits Gaussian behavior, and the intensity can be written

$$\lim_{p \rightarrow 0} \frac{I^G(\mathbf{Q})}{I_0^G(\mathbf{Q})} = \exp \left[-\frac{4\sigma_d^2}{c^0} \sin^2\left(\frac{Q_z c^0}{2}\right) \right] : \quad (12)$$

Equation 12 is applicable to continuous deposition methods, as well as the limit where scattered intensity becomes insensitive to the discrete nature of the surface roughness. For experimental

methods that are insensitive to the crystal miscut, equation 12 therefore also represents the appropriate model for continuous roughness, and is applicable anywhere along the CTR.

Having derived an expression for the influence of discrete roughness, we return our attention to the case where the surface height distribution is a continuous, multimodal function. The convolution of a binomial distribution defined by $n = 1$ and $p = 0.5$ with a Gaussian distribution will produce the surface height distribution shown in figure 2-(b). Using the convolution theorem, we now have a solution for the effects of the total surface roughness on the CTR intensity. The roughness has been parameterized into continuous and discrete contributions, which add in quadrature to yield the total surface roughness. For experimental methods that are insensitive to the crystal miscut, the total intensity including continuous and discrete contributions of roughness is written:

$$\frac{I(\mathbf{Q})}{I_0(\mathbf{Q})} = \left[1 - 4p(1-p)\sin^2\left(\frac{Q_z c^0}{2}\right) \right]^n \exp\left[-\frac{4\sigma_c^2}{c_0^2}\sin^2\left(\frac{Q_z c^0}{2}\right)\right] : \quad (13)$$

For miscut crystals where the intensity of a single CTR is measured, the total intensity is

$$\frac{I^G(\mathbf{Q})}{I_0^G(\mathbf{Q})} = \left[1 - 4p(1-p)\sin^2\left(\frac{Q_z c^0}{2}\right) \right]^n e^{-\sigma_c^2 (Q_z - G_z)^2} : \quad (14)$$

III. EXPERIMENTAL RESULTS

We used surface-sensitive X-ray scattering to study the $\text{h}001$ SrTiO_3 surface during annealing and homoepitaxy at the Cornell High Energy Synchrotron Source. Experiments were performed at the G3 hutch on the G-Line beamline. A double crystal synthetic multi-layer monochromator with 1.5% energy bandpass selected 10 KeV X-rays from the 48-pole wiggler spectrum, yielding 3×10^{11} photons/s/mm² at the sample. The spot size on the sample was set with 2 mm vertical by 0.5 mm horizontal slit immediately before the sample and the detector resolution was set with a 2 mm vertical by 0.5 mm horizontal slit at 600 mm from the sample.

A. Surface Roughening and Annealing

In order to grow epitaxial films of complex oxides, it is necessary to elevate the substrate temperature in order to enhance diffusion and reorganization of the adsorbed species. We have found that the $\text{h}001$ SrTiO_3 surface roughens during annealing to 300 °C. Figure 4 shows experimental specular CTR intensity data from two $\text{h}001$ SrTiO_3 samples under vacuum, one at room temperature (a), the other annealed at 300 °C (b). Both samples received a buffered HF etch treatment prior

to measurement.⁴⁰ The HF etch yields an atomically smooth TiO₂-terminated SrTiO₃ surface, with step edges that are one unit cell in height. During the heating process, we have observed a decline of CTR intensity in the $h00\frac{1}{2}i$ scattering geometry, which we attribute to an increased step edge density that may be related to a loss of oxygen from the SrTiO₃ surface.⁴¹ A least-squares fit for the room temperature data was performed using equation 12, yielding $\sigma_c = 1.52 \text{ \AA}$. The CTR intensity of the room temperature sample does not appear to be influenced by a discrete surface height distribution, as we would expect based on AFM results. The CTR intensity of the 300 C data, however, is very strongly influenced by discrete surface roughness; a least-squares fit was performed using equation 13, where $n = 1$, $p = 0.406$. The fit of the 300 C data yields a continuous roughness $\sigma_c = 0.715 \text{ \AA}$ and a discrete surface roughness of $\sigma_d = 1.917 \text{ \AA}$, yielding a total surface roughness of $\sigma = 2.05 \text{ \AA}$.

The temperature-dependent anti-Bragg scattering intensity for $h001i$ SrTiO₃ samples heated in 1×10^{-6} Torr O₂ through 0.3 Torr O₂ is presented in figure 5. As the temperature increased, the scattering intensity initially decreased due to increased surface roughness. The temperature corresponding to minimum scattering intensity varied with O₂ pressure: 250 C for 0.3 Torr, 350 C for 1×10^{-3} Torr, and 600 C for 3×10^{-6} Torr. As the temperature was increased further, the scattering intensity increased as the surface roughness decreased. Increasing the temperature in 0.3 Torr O₂ resulted in improved surface roughness at lower temperatures. The baseline error of the roughness determination in figure 5 is on the order of 10%, which dominates the determination of the errorbars. These results indicate that the surface roughness of $h001i$ SrTiO₃ can be improved by annealing at elevated temperature, and that ramping the substrate temperature in an appropriate O₂ pressure results in improved surface quality at lower temperatures.

In figure 6, an $h001i$ SrTiO₃ substrate was heated to 800 C in 1×10^{-6} Torr O₂. The scattered anti-Bragg intensity was monitored as a function of time, showing modest improvement of the surface roughness. After one hour, the O₂ pressure was increased to 1×10^{-3} Torr, resulting in a more rapid improvement of the scattered intensity and surface roughness. The total surface roughness in figures 5 and 6 does not approach zero, but a value corresponding to the roughness associated with the miscut. This result illustrates that at elevated temperatures, the use of an appropriate O₂ pressure causes the discrete roughness component to decrease at a faster rate, and that both continuous and discrete roughness should be considered during analysis.

B. Epitaxial Growth

Given an acceptable starting surface of $\text{h}001\text{i}$ SrTiO_3 , we can focus on homoepitaxial growth via PLD. A pulsed KrF excimer laser, with 248 nm wavelength and 30 ns pulse duration, was focused to provide a 200 MW/cm^2 power density at the surface of a single crystal SrTiO_3 target. The repetition rate was 0.03 Hz, and the growth rate was 0.08 monolayer/pulse. The substrate surface temperature was 550 C, and growth proceeded in a 0.02 Torr O_2 environment. Time-resolved X-ray CTR intensity measurements were made in the anti-Bragg scattering geometry in order to maximize sensitivity to surface roughness. PLD growth of $\text{h}001\text{i}$ SrTiO_3 in these conditions proceeds in a layer-by-layer growth mode, where many small two-dimensional islands nucleate, grow, and coalesce to form a complete overlayer. This type of growth gives rise to a strong discrete component of the surface roughness, which must be accounted for in order to fit the resulting oscillatory CTR intensity seen in the experimental data in figure 7(a).

The parameterization of roughness contributions in equation 14 enables a direct and simple method for analyzing scattering data from *in-situ* studies of film growth. The binomial distribution is used here to describe the state of the surface, not the physics of the adsorption and diffusion processes. In place of p , the fractional coverage per pulse, we use θ to define the fractional coverage of the growing layer. For ideal layer-by-layer growth, we set $n = \sigma_d^2 = \theta(1 - \theta)c^2 = 1$ always, and allow the coverage parameter θ to vary like a sawtooth waveform, where $0 \leq \theta \leq 1$. Since the scattered intensity depends on the quantity $\theta(1 - \theta)$ and not θ itself, we can equivalently define θ as a triangular waveform

$$\theta = \frac{1}{4} \frac{\sum_{j=0}^{\infty} \frac{\cos(2\pi j h k_i \pi)}{(2j+1)^2}}{\sum_{j=0}^{\infty} \frac{1}{(2j+1)^2}} + \frac{1}{5}; \quad (15)$$

where $0 \leq \theta \leq 0.5$ and $h k_i = h h_i = c^0$ is the normalized film thickness. In practice, neither layer completion nor half coverage occur at a specific moment across the entire sample, due to small position-dependent variations in the deposition rate. The series can be truncated at the first term to simulate this effect: $\theta = \cos(2\pi h k_i \pi) = 4.9352 + 1 = 4$.

As the film grows thicker and the continuous roughness increases due to the terraces become more and more irregularly shaped, we should expect that the influence of the discrete component will diminish. The decaying discrete roughness contribution is modeled using an effective coverage parameter $\theta^0 = \gamma \theta e^{-h k_i / \kappa}$, where $\gamma = 0.8$ and $\kappa = 18$. The presence of a characteristic thickness, κ , associated with the influence of discrete roughness provides a useful figure of merit for layer-by-

layer growth. Using scaling arguments described elsewhere,^{30,42} we have modeled the continuous roughness as a power-law $\sigma_c = \alpha k^{-\beta}$, with $\alpha = 0.617$ and $\beta = 0.34$. These models of the discrete, continuous, and total surface roughness as a function of film thickness is presented in figure 7(b). By considering both the discrete and continuous components, we obtain good agreement between experimentally measured scattered intensity and the model as seen in figure 7(a).

We have not observed a clear bimodal distribution in AFM data, even for post-deposition measurements of samples with many small two-dimensional islands or holes on the surface. In figure 2-(b), we show a hypothetical surface that exhibits a bimodal distribution, but we did not account for the effect of convoluting the AFM tip with the simulated morphology. Our AFM tips have a radius of approximately 10 nm, so it is not surprising that the AFM did not confirm the existence of the discrete roughness contribution. In this case, X-rays are more sensitive to such features.

IV. CONCLUSIONS

We have used surface-sensitive, incoherent X-ray diffraction for time-resolved studies of h001 SrTiO_3 surface morphology *in-situ*. Quantitative analysis of specular Crystal Truncation Rod intensity measurements require a model that is capable of handling the oscillatory surface roughness that occurs during layer-by-layer growth, as well as the non-periodic roughness that continues to accumulate with increasing film thickness. In general, the RMS surface roughness alone is not sufficient to model Crystal Truncation Rod intensity. Crystals with small terrace size relative to the coherence length exhibit concomitant discrete and continuous surface roughness, which we have modeled as a convolution of continuous and discrete distributions. The total surface roughness can then be parameterized into continuous and discrete roughness contributions, which add in quadrature. We derived a simple, closed-form expression for the scattering intensity which, for specific limiting cases, is equivalent to other models existing in the literature. This model is capable of handling smooth transitions between roughness that is discrete in nature to roughness that is continuous in nature, and therefore relaxes some of the restrictions of existing models of reflectivity.

We have observed good agreement between this model and experimental observations, allowing quantitative investigations of h001 SrTiO_3 annealing and thin film growth. We observed a surface roughening transition at temperatures that increased with decreasing O_2 pressure. The surface becomes smooth again as the temperature is further increased, and the rate of recovery was

improved by increasing the O₂ pressure. The maximum surface roughness observed during the annealing process was 2.05Å, and was primarily discrete in nature.

The continuous and discrete roughness parameters provide a useful method for analyzing *in-situ* scattering measurements of thin film growth. Growth of oxide thin films via Pulsed Laser Deposition tend to proceed with a layer-by-layer mechanism, which gives rise to a strong discrete roughness component that is periodic with film thickness. As the film continues to grow, we have observed an increase in the continuous roughness as well, which may be due to increasing irregularity of the terraces or surface relaxation. As the continuous roughness increases, the influence of the discrete roughness decreases. The decay rate of the discrete roughness contribution may serve as a useful figure of merit for describing layer-by-layer growth.

APPENDIX A

We offer an alternate derivation for the effect of a binomial surface height distribution. The specularly scattered amplitude from a perfectly flat substrate can be written

$$A_0 = \frac{F(Q_z)}{1 - e^{iQ_z c_0}}; \quad (\text{A1})$$

The scattering amplitude for an arbitrary surface, just before the n^{th} pulse, is

$$A_{n-1} = A_0 + \sum_{k=1}^n \theta_k F(Q_z) e^{iQ_z c_0 k}; \quad (\text{A2})$$

where θ_k is the fractional coverage of the k^{th} overlayer. In the case of random deposition, the amount of material depositing onto layer $k-1$ is equal to $p(\theta_{k-1} - \theta_k)$, where p is the fraction of the total surface covered by a single pulse. The scattering amplitude just after the n^{th} pulse is

$$\begin{aligned} A_n &= A_0 + \sum_{k=1}^n [p(\theta_{k-1} - \theta_k) + \theta_k] F(Q_z) e^{iQ_z c_0 k} \\ &= A_{n-1} - p \sum_{k=1}^n \theta_k F(Q_z) e^{iQ_z c_0 k} + p \sum_{k=1}^n \theta_{k-1} F(Q_z) e^{iQ_z c_0 k}; \end{aligned} \quad (\text{A3})$$

The second sum in equation A3 can be rewritten

$$\sum_{k=1}^n \theta_{k-1} F(Q_z) e^{iQ_z c_0 k} = e^{iQ_z c_0} F(Q_z) + \sum_{k=1}^n \theta_k F(Q_z) e^{iQ_z c_0 k}$$

such that, with some rearrangement, we can solve for I_n in terms of I_{n-1}

$$A_n = A_{n-1} - p \sum_{k=1}^n \theta_k F(Q_z) e^{iQ_z c_0 k}$$

$$\begin{aligned}
& + p e^{iQ_z c_0} F(Q_z) \frac{1}{1} \frac{e^{iQ_z c_0}}{e^{iQ_z c_0}} + \sum_{k=1}^n \theta_k F(Q_z) e^{iQ_z c_0 k} \\
& = A_{n-1} p \frac{1}{1} e^{iQ_z c_0} A_0 p \frac{1}{1} e^{iQ_z c_0} \sum_{k=1}^n \theta_k F(Q_z) e^{iQ_z c_0 k} \\
& = A_{n-1} \frac{1}{1} p + p e^{iQ_z c_0} \\
I_n & = I_{n-1} \frac{1}{1} 4p(1-p) \sin^2 \frac{Q_z c_0}{2} :
\end{aligned}$$

Starting from a perfect surface with no miscut, the intensity after n pulses of random deposition, where the fraction p_n of the surface covered during each pulse p_n may vary, is therefore

$$I_n = I_0 \prod_n \frac{1}{1} 4p_n(1-p_n) \sin^2 \frac{Q_z c_0}{2} : \quad (\text{A4})$$

ACKNOWLEDGMENTS

This work was funded by the Cornell Center for Materials Research (CCMR), which is supported by the National Science Foundation under award DMR-0079992, part of the NSF MRSEC Program. This work is based upon research conducted at the Cornell High Energy Synchrotron Source (CHESS) which is supported by the National Science Foundation and the National Institutes of Health/National Institute of General Medical Sciences under award DMR-0225180. Python and SciPy were used for data analysis, and Matplotlib was used to generate the figures herein. We wish to thank Arthur Woll for helpful discussions.

Electronic address: dd55@cornell.edu; Present Address: Cornell High Energy Synchrotron Source, Cornell University, Ithaca, New York 14853, USA

[†] Present Address: MIT Lincoln Laboratory, 244 Wood Street, Lexington, MA 02420, USA

¹ L. C. A. Stoop and J. H. Van Der Merwe, *Thin Solid Films* **17**, 291 (1973).

² F. Frank, *J. Cryst. Growth* **22**, 233 (1974).

³ G. Gilmer, *J. Cryst. Growth* **49**, 465 (1980).

⁴ W. van Saarloos and G. H. Gilmer, *Phys. Rev. B* **33**, 4927 (1986).

⁵ A. Ohtomo and H. Hwang, *Nature* **427**, 423 (2004).

⁶ T. Terashima, Y. Bando, K. Iijima, K. Yamamoto, K. Hirata, K. Hayashi, K. Kamigaki, and H. Terauchi, *Phys. Rev. Lett.* **65**, 2684 (1990).

- ⁷ H. Karl and B. Stritzker, Phys. Rev. Lett. **69**, 2939 (1992).
- ⁸ G. Koster, G. Rijnders, D. Blank, and H. Rogalla, Appl. Phys. Lett. **74**, 3729 (1999).
- ⁹ A. Ohtomo, D. Muller, J. Grazul, and H. Hwang, Nature **419**, 378 (2002).
- ¹⁰ A. Fleet, D. Dale, Y. Suzuki, and J. D. Brock, Phys. Rev. Lett. **94**, 036102 (2005).
- ¹¹ A. Fleet, D. Dale, A. R. Woll, Y. Suzuki, and J. D. Brock, Phys. Rev. Lett. **96**, 055508 (2006).
- ¹² D. W. Kisker, G. B. Stephenson, J. Tersoff, P. H. Fuoss, and S. Brennan, J. Cryst. Growth **163**, 54 (1996).
- ¹³ R. L. Headrick, S. Kycia, Y. K. Park, A. R. Woll, and J. D. Brock, Phys. Rev. B **54**, 14686 (1996).
- ¹⁴ M. V. Ramana Murty, T. Curcic, A. Judy, B. H. Cooper, A. R. Woll, J. D. Brock, S. Kycia, and R. L. Headrick, Phys. Rev. B **60**, 16956 (1999).
- ¹⁵ G. Eres, J. Z. Tischler, M. Yoon, B. C. Larson, C. M. Rouleau, D. H. Lowndes, and P. Zschack, Appl. Phys. Lett. **80**, 3379 (2002).
- ¹⁶ E. Vlieg, A. W. Denier van der Gon, J. F. van der Veen, J. E. Macdonald, and C. Norris, Phys. Rev. Lett. **61**, 2241 (1988).
- ¹⁷ P. H. Fuoss, D. W. Kisker, F. J. Lamelas, G. B. Stephenson, P. Imperatori, and S. Brennan, Phys. Rev. Lett. **69**, 2791 (1992).
- ¹⁸ A. R. Woll, R. L. Headrick, S. Kycia, and J. D. Brock, Phys. Rev. Lett. **83**, 4349 (1999).
- ¹⁹ P. R. Willmott, R. Herger, C. M. Schlepütz, D. Martoccia, and B. D. Patterson, Phys. Rev. Lett. **96**, 176102 (2006).
- ²⁰ J. Z. Tischler, G. Eres, B. C. Larson, C. M. Rouleau, P. Zshack, and D. H. Lowndes, Phys. Rev. Lett. **96**, 226104 (2006).
- ²¹ K. Iijima, T. Terashima, Y. Bando, K. Kamigaki, and H. Terauchi, J. Appl. Phys. **72**, 2840 (1992).
- ²² T. Tsurumi, T. Suzuki, M. Yamane, and M. Daimon, Jpn. J. Appl. Phys. **33**, 5192 (1994).
- ²³ H. Tabata, H. Tanaka, and T. Kawai, Appl. Phys. Lett. **65**, 1970 (1994).
- ²⁴ R. Takahashi, Y. Matsumoto, H. Koinuma, M. Lippmaa, and M. Kawasaki, Appl. Surf. Sci. **197**, 532 (2002).
- ²⁵ G. Koster, K. Verbist, G. Rijnders, H. Rogalla, G. van Tendeloo, and D. Blank, Physica C **353**, 167 (2001).
- ²⁶ T. Tsurumi, T. Harigai, D. Tanaka, S.-M. Nam, H. Kakemoto, S. Wada, and K. Saito, Appl. Phys. Lett. **85**, 5016 (2004).
- ²⁷ H. N. Lee, H. Christen, M. Chisholm, C. Rouleau, and D. Lowndes, Nature **433**, 395 (2005).
- ²⁸ B. Vidal and P. Vincent, Applied Optics **23**, 1794 (1984).

- ²⁹ C. Lent and P. Cohen, Surf. Sci. **139**, 121 (1984).
- ³⁰ H.-N. Yang, G.-C. Wang, and T.-M. Lu, *Diffraction from Rough Surfaces and Dynamic Growth Fronts* (World Scientific Publishing Co., 1993), and references therein.
- ³¹ D. Gibbs, B. M. Ocko, D. M. Zehner, and S. G. J. Mochrie, Phys. Rev. B **38**, 7303 (1988).
- ³² E. D. Specht and F. J. Walker, J. Appl. Crystallogr. **26**, 166 (1993).
- ³³ B. E. Warren, *X-ray Diffraction* (Dover Publications, 1990).
- ³⁴ S. K. Sinha, E. B. Sirota, S. Garoff, and H. B. Stanley, Phys. Rev. B **38**, 2297 (1988).
- ³⁵ G. A. Held and J. D. Brock, Phys. Rev. B **51**, 7262 (1995).
- ³⁶ J. Pimbley and T.-M. Lu, J. Vac. Sci. Technol. A **2**, 457 (1984).
- ³⁷ S. Andrews and R. Cowley, J. Phys. C **18**, 6427 (1985).
- ³⁸ S. Sinha, Y. Feng, C. Melendres, D. Lee, T. Russell, S. Satija, E. Sirota, and M. Sanyal, Physica A **231**, 99 (1996).
- ³⁹ I. K. Robinson, Phys. Rev. B **33**, 3830 (1986).
- ⁴⁰ M. Kawasaki, K. Takahashi, T. Maeda, R. Tsuchiya, M. Shinohara, O. Ishiyama, T. Yonezawa, M. Yoshimoto, and H. Koinuma, Science **266**, 1540 (1994).
- ⁴¹ M. Lippmaa, M. Kawasaki, A. Ohtomo, T. Sato, M. Iwatsuki, and H. Koinuma, Appl. Surf. Sci. **132**, 582 (1998).
- ⁴² A.-L. Barabasi and H. E. Stanley, *Fractal Concepts in Surface Growth* (Cambridge University Press, 1995).

Figure 1: (a) Simulated reciprocal space map ($H = 0$) of intensity for a TiO_2 terminated SrTiO_3 substrate with 0.198° miscut in the $h0K0i$ direction. The transverse coherence length is assumed to be $1\mu\text{m}$. (b) Experimental K -scan data from a $h001i$ SrTiO_3 substrate, $H = 0; L = 0.5$. The scattering power is normalized to the total incident power. The grey line is simulated with the kinematic scattering theory.

Figure 2: (a) AFM image of a SrTiO_3 substrate. Inset: Histogram of the surface height distribution, with a Gaussian fit. The RMS roughness is 1.44 \AA . (b) Using image (a), simulation of random deposition of one half monolayer.

Figure 3: Calculated intensity along the specular CTR. For $n=0$, no material has been deposited and the substrate is ideally flat. For one pulse that covers half of the flat surface with new material, complete destructive interference is observed in the anti-Bragg scattering geometries. A nearly identical RMS surface roughness is observed for 25 pulses each randomly covering 1% of the surface with new material, but the RMS surface roughness alone is not sufficient to model the CTR intensity profile.

Figure 4: Reflectivity data for $h001i$ SrTiO_3 prepared with buffered-HF etch. The orientation of the miscut, and the resulting truncation rod splitting, were integrated by the resolution function. (a) 25° C , $4 \times 10^{-7} \text{ Torr}$. (b) 300° C , $1 \times 10^{-5} \text{ Torr}$.

Figure 5: X-ray scattering studies of SrTiO_3 surface vs. temperature. (a) $h00\frac{1}{2}i$ scattering intensity vs. temperature. (b) RMS surface roughness vs. temperature, as determined from the scattering intensity.

Figure 6: X-ray scattering measurement of SrTiO_3 surface vs. time. The sample temperature is 800° C , and the O_2 pressure is increased from $1 \times 10^{-6} \text{ Torr}$ to $1 \times 10^{-3} \text{ Torr}$ after one hour. (a) $h00\frac{1}{2}i$ scattering intensity vs. temperature. (b) RMS surface roughness vs. temperature, as determined from the scattering intensity.

Figure 7: Anti-Bragg X-ray scattering measured *in-situ* during $h001i$ SrTiO_3 homoepitaxy via PLD. (a) Growth oscillations measured in the $h00\frac{1}{2}i$ scattering geometry. The model uses the roughness depicted in (b), where the total surface roughness includes both continuous and discrete contributions, which add in quadrature.

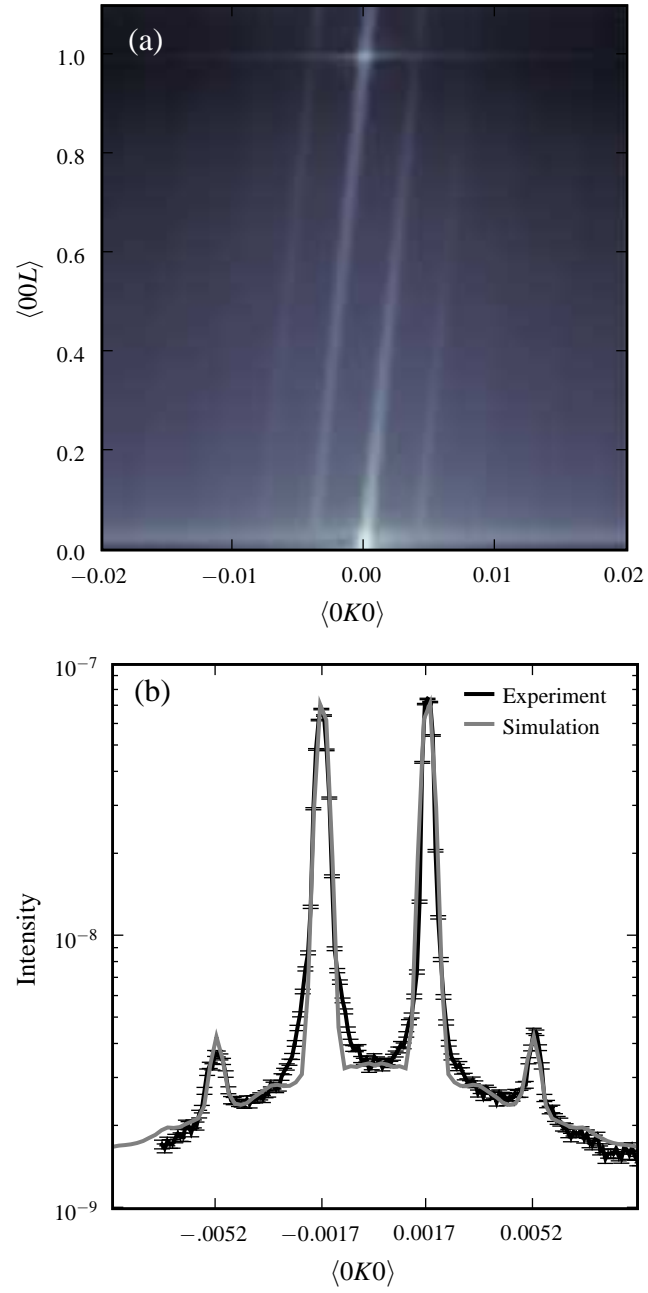


FIG. 1: Darren Dale, Physical Review B

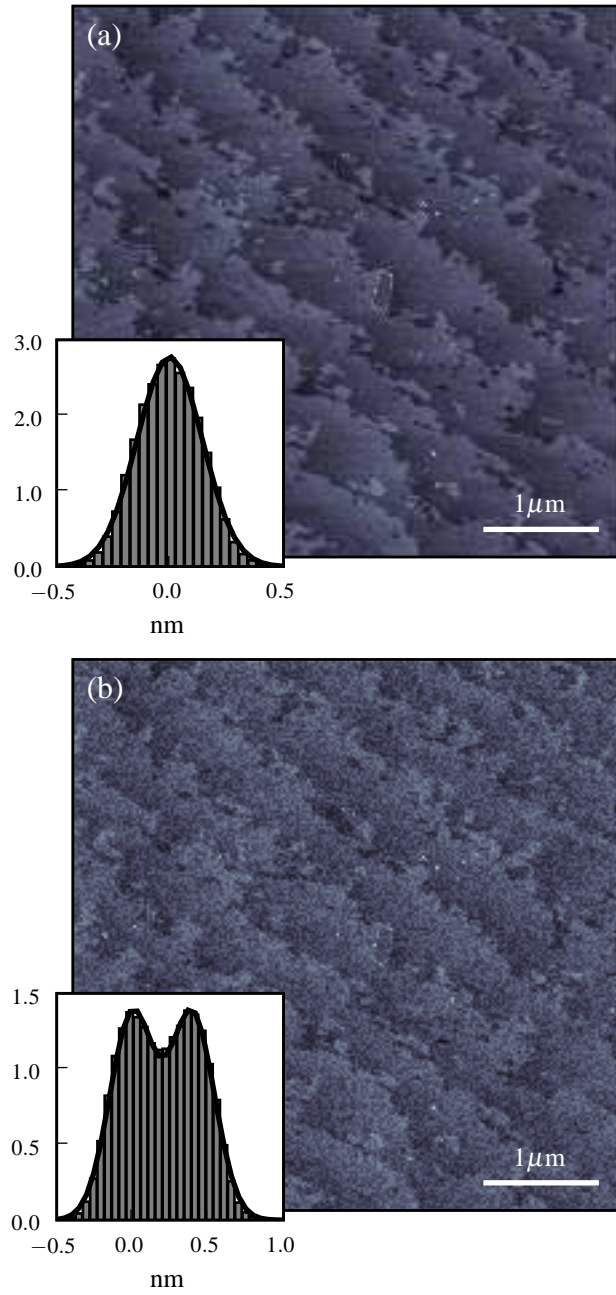


FIG. 2: Darren Dale, Physical Review B

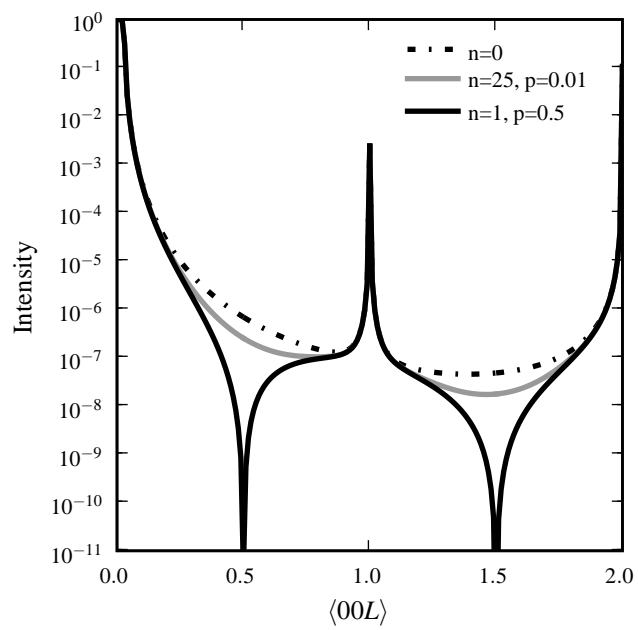


FIG. 3: Darren Dale, Physical Review B

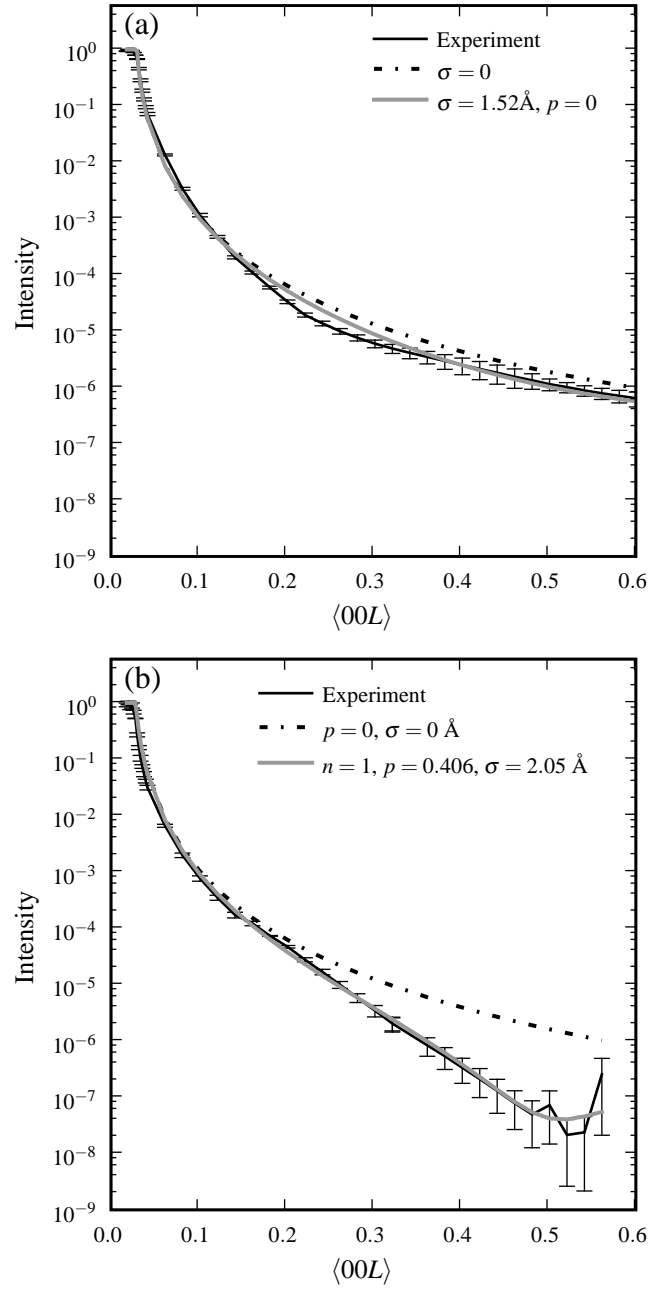


FIG. 4: Darren Dale, Physical Review B

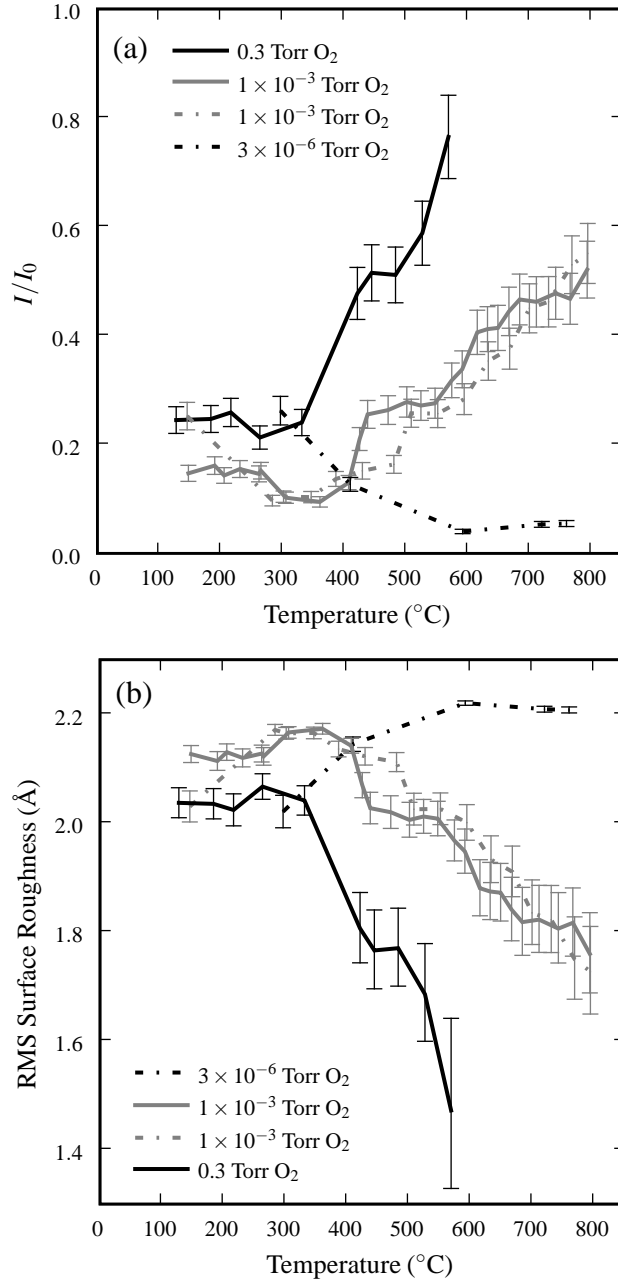


FIG. 5: Darren Dale, Physical Review B

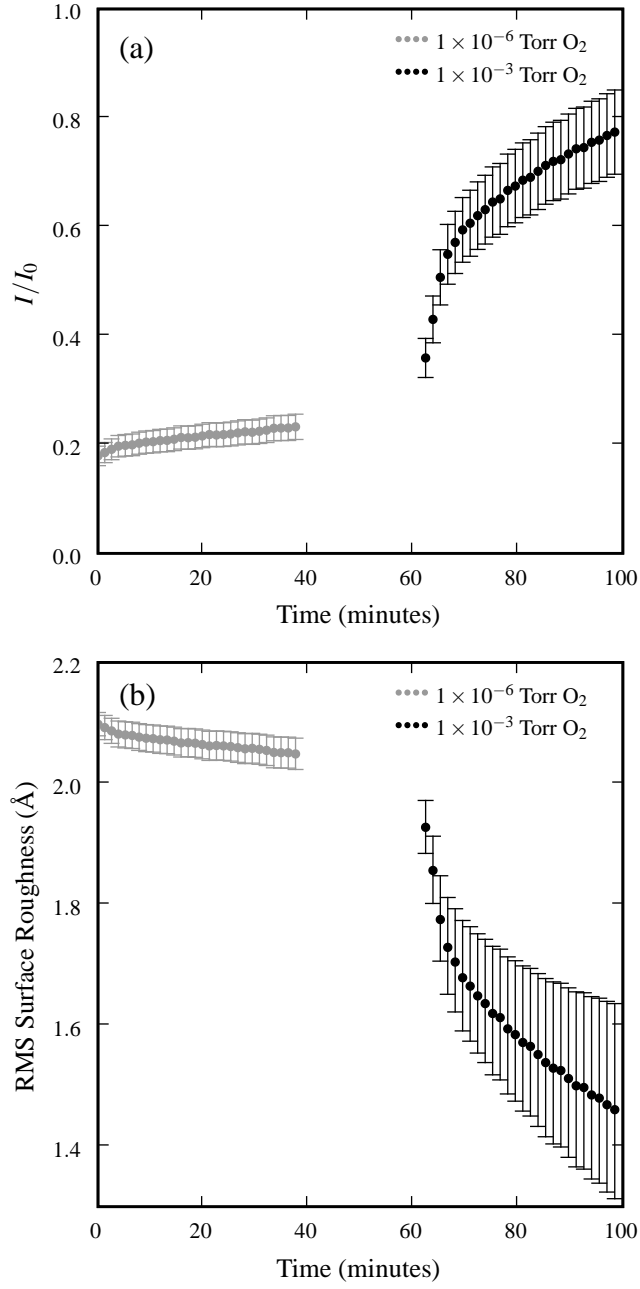


FIG. 6: Darren Dale, Physical Review B

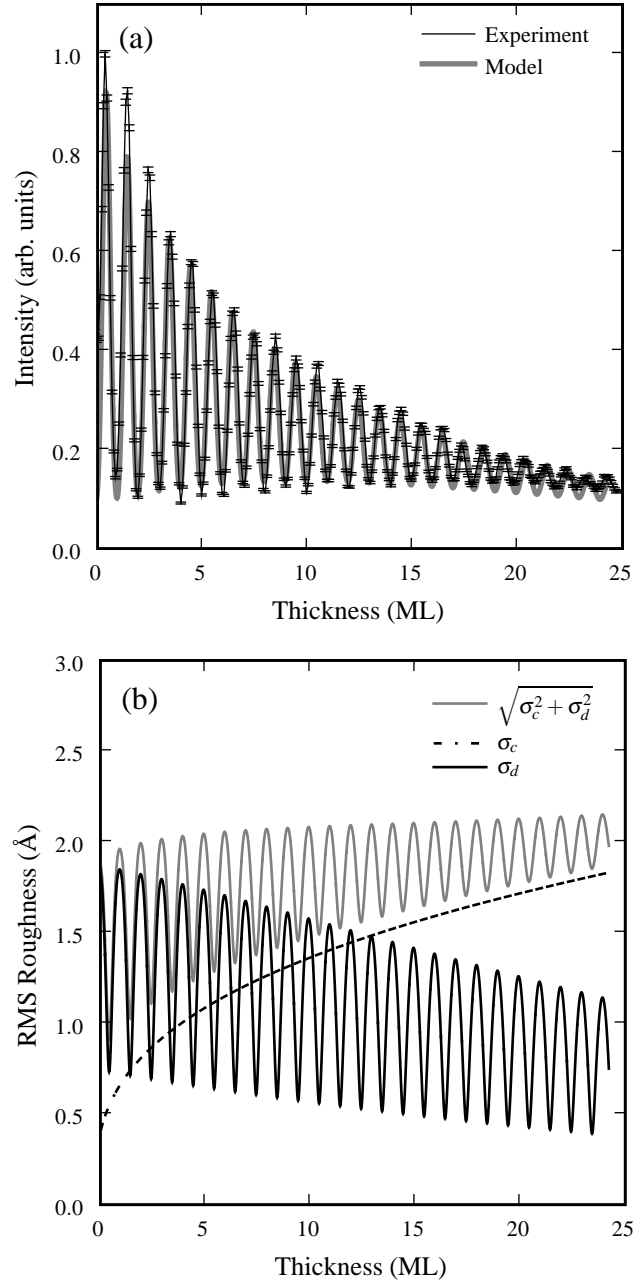


FIG. 7: Darren Dale, Physical Review B